Journal of the Mechanical Behavior of Biomedical Materials 71 (2017) 416–427

Contents lists available at ScienceDirect

Journal of the Mechanical Behavior of Biomedical Materials

journal homepage: www.elsevier.com/locate/jmbbm

Modelling dental implant extraction by pullout and torque procedures

D. Rittel*, A. Dorogoy, K. Shemtov-Yona

Faculty of Mechanical Engineering Technion, 32000 Haifa, Israel

ARTICLE INFO

Keywords:
Dental implant
Extraction
Torque
Load
Numerical modelling

ABSTRACT

Dental implants extraction, achieved either by applying torque or pullout force, is used to estimate the bone–implant interfacial strength. A detailed description of the mechanical and physical aspects of the extraction process in the literature is still missing.

This paper presents 3D nonlinear dynamic finite element simulations of a commercial implant extraction process from the mandible bone. Emphasis is put on the typical load-displacement and torque-angle relationships for various types of cortical and trabecular bone strengths. The simulations also study of the influence of the osseointegration level on those relationships. This is done by simulating implant extraction right after insertion when interfacial frictional contact exists between the implant and bone, and long after insertion, assuming that the implant is fully bonded to the bone. The model does not include a separate representation and model of the interfacial layer for which available data is limited.

The obtained relationships show that the higher the strength of the trabecular bone the higher the peak extraction force, while for application of torque, it is the cortical bone which might dictate the peak torque value. Information on the relative strength contrast of the cortical and trabecular components, as well as the progressive nature of the damage evolution, can be revealed from the obtained relations. It is shown that full osseointegration might multiply the peak and average load values by a factor 3–12 although the calculated work of extraction varies only by a factor of 1.5.

From a quantitative point of view, it is suggested that, as an alternative to reporting peak load or torque values, an average value derived from the extraction work be used to better characterize the bone–implant interfacial strength.

1. Introduction

Osseointegration is defined as “direct structural and functional connection between ordered, living bone and the surface of a load-carrying implant” (Albrektsson et al., 1981; Stanford and Keller, 1991). This process can be regarded as a bone healing process, which creates a biological fixation through continuous bone apposition and remodeling towards the implant.

This dynamic process, that takes place at the interface between the solid implant and the biological hard tissue, depends on various factors, such as the implant's biomaterial and surface composition, topography, implant geometry, fixation type, and of course healing time after implant placement. In addition, several patient factors also contribute to the success of the process, such as the patient's medical condition (diabetes, bone disease, medication), oral habits (clenchers and bruxers), and of course the surgical protocol.

Several methods exist in order to evaluate the quality and quantity of osseointegration and the interfacial bond between the implant and the host bone (Atsumi et al., 2007). Although histological analysis is regarded as the gold standard to evaluate the degree of osseointegration, several biomechanical test methods have been developed, such as the “push out”, “pullout” and “torsion” tests. These can be used to test the *ex vivo* mechanical state of biological fixation of the implant through the evaluation of the shear strength of the bone implant interface (Chang et al., 2010).

The “push out/pullout test” is also a commonly used approach to investigate the interfacial stiffness. In a typical test, a cylindrical implant is placed in bone structures, and then removed after predetermined healing time by applying a force along the implant's longitudinal axis. The interfacial stiffness can be approximated using the force–displacement curve obtained during the test (Brunski et al., 2000; Chang et al., 2010a, 2010b). This method is more suitable to cylindrical type implants. The pullout test is recommended by ASTM F543-07 (American Society for Testing and American Society for Testing and Materials, 2009), as the standard method to simulate the axial withdrawal of a screw from the cadaveric or synthetic bone. The screw

* Corresponding author.
E-mail address: merittel@technion.ac.il (D. Rittel).

http://dx.doi.org/10.1016/j.jmbbm.2017.04.010
Received 13 February 2017; Received in revised form 27 March 2017; Accepted 10 April 2017
Available online 11 April 2017

withdrawal process is recorded as a load–displacement curve, and the holding power is defined as the peak value of the load–displacement curve (Hou et al., 2004; Hsu et al., 2005; Huja et al., 2005). This peak value is considered as an estimate the bone–screw interfacial strength (Hoshaw et al., 1994).

During a "torque test", the implant is unscrewed and the removal torque values are recorded (Trisi et al., 2011). Using this approach, interfacial shear properties are measured (Atsumi et al., 2007; Chang et al., 2010), and a torque–angle curve is obtained. This method is more suitable to screw type implants.

These mechanical tests have been used in implant dentistry to investigate the healing capabilities at the bone implant interface, with emphasis on the effect of healing time (Brånemark et al., 1997, 1998; Kraut et al., 1991), or the effect of the surface treatment (condition) (Ferguson et al., 2008).

Brånemark et al. (1997, 1998) were among the first to evaluate the biomechanics of titanium implants in animal models (rats and dogs) after varying periods of healing without loading (submerged), by *ex-vivo* torsion tests, pull-out tests, and histological analysis. Their detailed studies showed a clear correlation between the shear stresses and shear moduli in the bone tissue (pull-out test), and at the interface (torque test), and bone-implant contact area. As the duration of the bone healing increases, a substantial improvement in the mechanical shear response could be observed.

Ferguson et al. (2008) performed a biomechanical study evaluating the effect of various surface treatments, conventional (sandblasting and etching, CaP coated and anodized), and alternative treatments (coating with bisphosphonate or artificial extracellular matrix) on osseointegration. The healing process was evaluated using in-vivo animal sheep model. Peri-implant bone density and removal torque were compared at 2, 4, and 8 weeks after implantation. A torque-rotation curve was constructed and the maximum removal torque (N-mm) value was recorded. Interestingly, bone-implant interfacial failure could be qualitatively distinguished by 3 different kinds of torque-angle relationship, with each surface treatment characterized by a specific tendency.

Here, one should note that the force needed to either push out or pull out an implant specimen is mostly borne by the interfacial area. Therefore, while the assumption of an "average shear stress" may be applicable to a regular cylindrical specimen, the more complex realistic implant geometry with its threads renders this notion questionable for the simple reason that neither the interfacial stresses or strains are homogeneous anymore.

From the above-mentioned references, it seems that because of variability in test conditions and parameters, the reported test results are quite scattered, so that one cannot *systematically* compare the interfacial stiffness or shear properties and draw firm conclusions.

Numerical models are used extensively in medicine and in dentistry in order to simulate a medical device and evaluate its behavior in a tested environment, under a predetermined set of selected model parameters. These "in silico" methods, which are more controlled and unlimited in terms of test/model parameters, provide valuable insight on mechanical behavior of the device. While there is a very large number of papers about numerical modeling of the bone-implant interaction, with emphasis on local strains, stresses and bone remodeling to some extent, papers reporting models of implant pullout, pushout or torque tests, with emphasis on the bone-implant interface are still quite scarce.

Dhert et al. (1992) used finite element modelling to evaluate the interfacial stress distribution on a stem implant used in orthopedics and placed solely in the cortical bone. This early frictionless numerical model used rather simplistic assumptions to calculate the mean interfacial strength without showing the evolution of the process at the bone level in terms of damage for instance.

Hansson et al. (2011) developed an analytical model for the interfacial strength of a rough cylinder based on strength of materials considerations, into which surface roughness elements were included to enhance the physical aspects of the problem. This study did not account for the geometry of a real dental implant with its threads. Mathieu et al. (2012) recently evaluated experimentally, and then modelled the interfacial strength and fracture behavior of the bone-implant system, for a coin-shaped implant, using analytical fracture mechanics concepts. This work addressed specifically torque tests to which mode III fracture is particularly suitable, while paying attention to the cohesive/adhesive nature of the failure process which is seldom addressed in this context. Additional studies reported a high correlation between the numerical indices and measured holding power, see e.g. (Hou et al., 2004; Hsu et al., 2003, 2005).

This literature survey shows that the few experimental studies are essentially aimed at estimating an averaged value of the bone-implant interfacial strength based on homogeneity assumptions that may be questionable. The few available analytical studies correlate the experimentally measured parameters to the interfacial strength and failure parameters of geometrically simplified models. Moreover, there is an even greater scarcity of numerical models for those complex tests, in which a minimal number of assumptions are made, that could provide information on both the mechanical strength parameters and also on the evolution of the physical damage processes that lead to implant total extraction. The complete simulation of a *real implant geometry* being pulled or torque-extracted is still missing.

This numerical study addresses the extraction process of a dental implant by pullout and torque procedures. Specifically, we study the effect of osseointegration on the extraction process by modeling two limit cases: 1) Extraction immediately after insertion (no osseointegration). 2) Extraction after a long time, where the implant is fully osseointegrated and thus fully bonded to the bone.

The pullout results for a wide range trabecular bone parameters, right after insertion are presented first. The results by pulling and torque of an osseointegrated implant are shown next, followed by a comparative and a sensitivity analysis of the torque to various material parameters. A discussion and conclusion section end this manuscript.

2. Material and methods

The extraction process of the representative commercial implant (shown in Fig. 1) from the mandible bone, was simulated numerically (Simulia, 2014a). Two extraction procedures were modelled:

1) Straight implant pullout (pullout).
2) Rotational un-screwing (torque).

The following two cases were considered:

a) The implant was extracted immediately after insertion. In that case, the only interaction between the bone and the implant is frictional.
b) The implant was extracted "sufficiently long" after insertion, so that full osseointegration had taken place. Here, perfect bonding was assumed.

The two cases and their associated extraction procedures are summarized in Table 1. The torque process was not simulated for case (a) because the calculated torque value is very small, and thus of limited interest.

2.1. Pullout of a rigid implant right after insertion

This simulation is a direct continuation of our previous work (Dorogoy et al., 2017), in which the *insertion* process was modeled in detail. Here too, the model is three-dimensional, and the analyses are dynamic, continuous and non-linear. The implant is modeled as a rigid structure. The simulations were performed in three steps:

Fig. 1. a. The MIS SEVEN implant: 3.75 mm diameter, 13 mm length. Reprinted from: http://www.misimplants.com/implants/brands/seven/seven-mf7-13375.html.

2.1.1. Insertion

The insertion step is identical to that described in Dorogoy et al. (2017) and will not be described here.

2.1.2. Rest

The purpose of the “rest” phase was to let dynamic effects, which might exist due to the dynamic solution process, fade away.

2.1.3. Extraction

Pullout: The implant was pulled out at an average velocity of 15 mm/s. A displacement of 3 mm was applied with a smooth step (Simulia, 2014b) of 0.2 s. It was verified that the inertial dynamic effects are negligible.

The finite element model, material models and mesh properties are fully detailed in Dorogoy et al. (2017), and are shown again in Appendix A just for the sake of completeness. The "rest" and "extraction" phases were simulated by restarting the calculations after the “insertion” step described in Dorogoy et al. (2017).

During the rest phase, once the implant was fully inserted, no load was applied on the implant and its displacements were kept to zero.

For the pullout procedure, the rigid implant was only allowed to move upwards in the y direction. A cross-sectional view through the implant and bone at the end of the "rest" step, just before "extraction", is shown in Fig. 2. The residual von Mises stress distribution due to the insertion process is clearly visible. Note that this procedure is applied as a “restart” of the insertion state, with the current state of damage and residual stresses. Here, according to our previous work on implant insertion (Dorogoy et al., 2017), the cortical bone thread was severely damaged by the implant's micro-grooves.

Table 1
The two cases and their associated extraction procedures.

	No osseointegration	Osseointegration
Straight implant pullout (pullout)	√	√
Rotational un-screwing (torque)	X	√

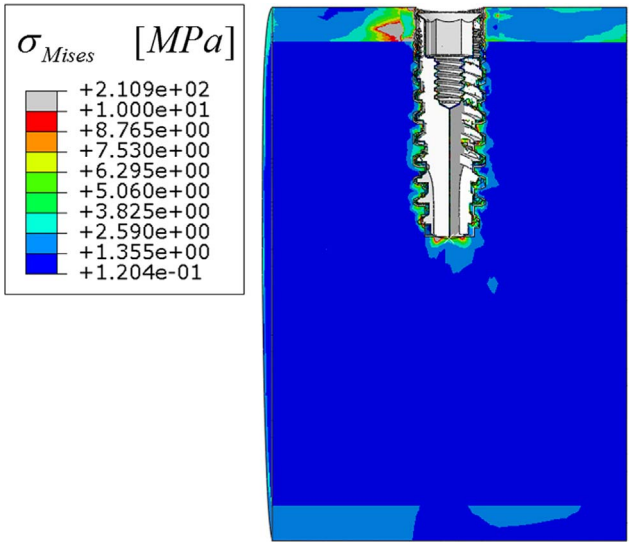

Fig. 2. A cross-sectional view through the implant and bone, showing the residual Mises stress distribution at the end of the rest step, just before the restart phase. Note that the cortical bone thread has been severely damaged by the implant's micro-grooves (Dorogoy et al., 2017).

By contrast, when the osseointegrated state was simulated, the system had no residual stresses or damage whatsoever, as it was assumed that bone healing had created a completely new state in which the implant and the bone are now fully bonded.

During all three steps the general contact algorithm of Abaqus (Simulia, 2014b) was used. The algorithm uses element-based surfaces, which can adapt to the exposed surfaces of the current non-failed elements. Abaqus' frictional tangential behavior with the penalty formulation was adopted. A frictional Coulomb contact was used with a constant coefficient of friction 0.61 (Grant et al., 2007; Guan et al., 2011). All the surfaces that may become exposed during the analysis, including faces that are originally in the interior of bone, were included in the contact model. We assumed that contact nodes still take part in the contact calculations, even after all of the surrounding elements have failed. These nodes act as free-floating point masses that can experience contact with the active contact faces.

2.2. Pullout and unscrewing of fully bonded titanium implant

It is assumed that a “long time” has elapsed since the insertion of the implant, and the bone has fully recovered. Osseointegration has taken place and the implant is fully bonded to the surrounding bone, and all damage has “healed” due to osseointegration. The only difference with respect to Section 2.1 is that the implant is no longer rigid, but is made of titanium alloy (Ti6Al4V), and is fully inserted within the bone prior to load application. The Ti6Al4V was modeled as an elastic material, and its parameters are given in Table 2. Usage of Ti6Al4V instead of a rigid material for the insertion step would have resulted in a much higher computation time (which is already high), without significant effect on the insertion torque. Since the pullout step is rather short in time, it was decided a model the implant as a “true” elastic material.

2.2.1. Assembly

The full assembly, which comprises of all fully bonded cortical bone (red), trabecular bone (green) and Ti6Al4V implant (gray), is shown in

Table 2
Material properties of Ti6Al4V.

ρ [Kg/m^3] density	E [MPa] Young's modulus	ν Poisson's ratio	σ_Y [MPa] yield stress
4430	11,380	0.342	880

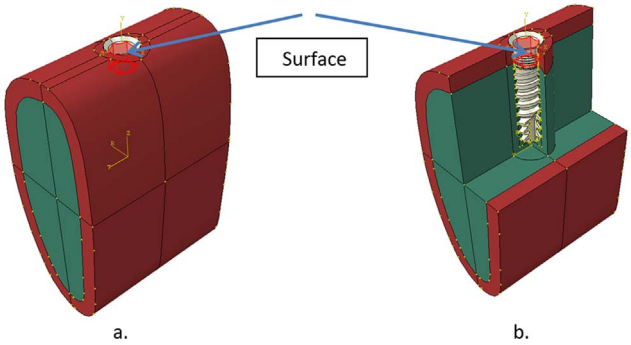

Fig. 3. The assembly. a. full assembly. b. Inner structure of the assembly. Note the surface on which load is applied. The inner surface is marked IS. (For interpretation of the references to color in this figure, the reader is referred to the web version of this article).

Fig. 3a. In Fig. 3b, part of the model has been removed to reveal the internal assembly of the bone and the implant. Loads were applied on the inner surface (IS) shown in Fig. 3a, b.

2.2.2. Mesh and boundary conditions

The mesh is shown in Fig. 4. Here too, parts of the model have been removed to show the mesh of the implant and its surroundings, which have a dense mesh of 0.1–0.2 mm seed size. The mesh comprises 1,283,608 linear tetrahedral elements of type C3D4. The boundary conditions on the bone are identical to those of Section 2.1.

For pulling out the implant, an average velocity of 15 mm/s was applied to the IS shown in Fig. 3a, b and 5b. The velocity is the same as for immediate extraction. For unscrewing the implant, a rigid screwdriver was added to the assembly as shown in Fig. 5. A constant rotational velocity of 6.28 rad/s was applied to the reference point of the rigid screwdriver as shown in Fig. 4a. The load was inserted by

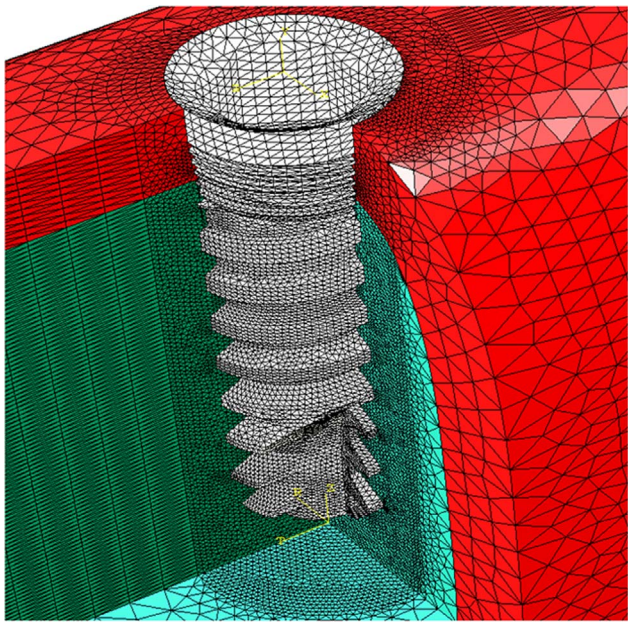

Fig. 4. Inner view of the mesh.

frictional contact between the outer surface of the rigid screwdriver and the inner surface of the implant (IS) shown again in Fig. 5b. An upward vertical load of 6 N was applied to the implant at 6 points as shown in Fig. 5c.

3. Results

3.1. Pullout of a rigid implant right after insertion

Five types of trabecular bones, which differ in their yield stress, were tested, namely $\sigma_y = 10$, 20, 32, 47 and 62 MPa, respectively. Fig. 6 shows the resisting force to pulling versus the applied displacement. The curves are all similar: the load first increases with vertical displacement and reaches its maximum value at 0.2–0.4 mm. Thereafter, it gradually decreases and reaches zero at 1.0–1.2 mm. The higher the yield stress of the trabecular bone, the higher the peak value of the load. For $\sigma_y = 62$ MPa $P_{peak} \sim 1200$ N, while for $\sigma_y = 10$ MPa $P_{peak} \sim 200$ N.

3.2. Extraction of fully bonded titanium implant

3.2.1. Pullout of fully bonded titanium implant

Fig. 7 shows the calculated resisting force versus the vertical displacement of the IS of the implant for the above-mentioned five types of trabecular bones.

All curves behave again the same up to ~0.05 mm, where a local peak force is observed. Immediately past this peak, the force drops and reaches a local minimum value. With increasing displacement, the force increases again up to a second peak, and then drops rapidly to zero. While the first peak force is identical to all types of trabecular bones, the second one (P2) is different. The higher the yield stress, the higher P2. For $\sigma_y = 62$ MPa P2 ~3700 N while for $\sigma_y = 10$ MPa P2~1000 N. While for $\sigma_y = 62$ MPa the resisting force drops to zero at a vertical displacement of 0.27 mm, it does so at 0.18 mm for $\sigma_y = 10$ MPa. All in all, it can be noted that irrespective of the bone strength parameters, a very small vertical displacement is sufficient to detach the implant from the bone to a point that the interaction between the two no longer exists.

The extraction process is illustrated in Fig. 8. A cross-sectional view through the bone where the titanium implant is removed is shown in Fig. 8a. The trabecular yield stress is 32 MPa. In Fig. 8a, the cortical bone and the trabecular bone have different colors. Fig. 8b-e show the deformed bone with equivalent plastic strain distribution at different vertical displacements. Fig. 8b shows the progress of the plastic deformation at 0.06 mm. Fig. 8c shows it at 0.13 mm. The plastic deformation and detachment/debonding continues to propagate deep into the trabecular bone as shown in Fig. 8d for 0.162 mm. At a vertical displacement of 0.20 mm, the implant is fully debonded, as shown in Fig. 8e. The torn bone parts that are attached to the implant and move upward with it, are shown in Fig. 8f at 1.5 mm upward vertical displacement. In Fig. 8f the colors indicate different vertical displacement.

3.2.2. Unscrewing of fully bonded titanium implant

Fig. 9 shows the calculated resisting torque versus the rotation angle of the reference point of the screwdriver shown in Fig. 5a. It is shown for the five above-mentioned types of trabecular bone strengths. The resisting torque is integrated by Abaqus over the inner surface of the implant (IS) shown in Fig. 5b and Fig. 3a, b.

It can be observed that up to $\theta = 3^\circ$, the torque resistance for all bones is identical: it reaches a peak of ~4700 Nmm, then drops abruptly to a lower value of ~800 Nmm. Increasing the rotation angle results in increased resisting torque up to a second peak. Further increase of the rotation angle causes a steep decrease in the torque, which then drops rapidly to zero. The angle (θ) and value of the second torque peak depend markedly on the trabecular yield stress. For

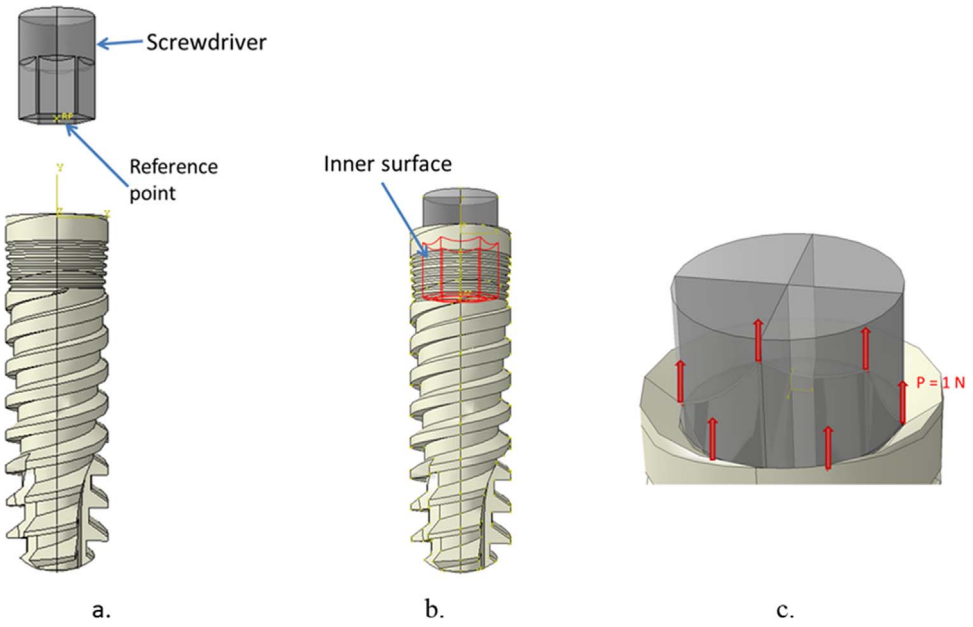

Fig. 5. Assembly of the rigid screwdriver and the titanium implant. a. Before assembly. Notice the reference point. b. After assembly. c. Location of 6 vertical loads of 1 N.

$\sigma_Y = 10$ MPa this second peak is located at $\theta = 4^\circ$ with a value of 1600 Nmm, while for $\sigma_Y = 62$ MPa, it is located at $\theta = 14.5^\circ$, with a peak value of 4600 Nmm. The first peak is always higher than the second.

The bone behavior during the unscrewing process is shown in Fig. 10. The trabecular bone has a yield strength $\sigma_Y = 32$ MPa and the applied angular velocity is 30 rpm. The figure shows a cross-sectional view through the bone, where both the titanium implant and the screwdriver are removed. Fig. 10a shows the bone prior to load application, with a differentiation between the cortical (red) and trabecular (green) zones. Fig. 10b-e show the deformed and damaged bone for increasing rotation angles. Fig. 10b shows the damage and debonding at $\theta = 3.2^\circ$. It can be observed that the upper zone (cortical bone) is first damaged. Fig. 10c-d, at $\theta = 5.0^\circ$ and $\theta = 6.8^\circ$ respectively, show that the damage and debonding are progressing along the implant. At $\theta = 8.3^\circ$ (Fig. 10f) the damage has reached the bottom of the implant, and the latter is now fully detached. At that angle, the upward forces (shown in Fig. 5c) start to pull the implant upward. At $\theta = 18^\circ$ (Fig. 10f) it can be observed that fragments of torn bone (all yellow) are moving upward with the implant.

3.3. Comparison between extraction procedures for various post- insertion times

3.3.1. Work considerations

The work done by the force to pullout the implant can be calculated by Eq. (1):

$$W_P = \int_0^{\Delta_f} P \, du \tag{1}$$

Where P is the applied force and u is the upward displacement. The displacement at which the load drops to zero is denoted by Δ_f.

The work done by the moment to unscrew the implant can be calculated by Eq. (2):

$$W_M = \int_0^{\theta_f} M \, d\theta \tag{2}$$

where M is the applied moment and θ is the rotation angle. The angle at which the moment drops to zero is denoted by θ_f.

The work for pulling out an implant immediately after insertion was calculated by application of Eq. (1) to the curves of Fig. 6. The work for

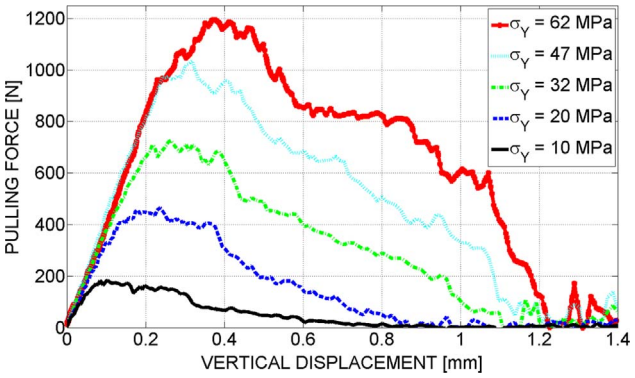

Fig. 6. Pulling force right after insertion, versus applied vertical displacement for 5 different yield stresses of the trabecular bone: 10, 20, 32, 47, and 62 MPa. Note the overall similarity of the curves. Since the cortical bone thread was damaged during the insertion phase, the mechanical contribution is mainly due to the trabecular bone.

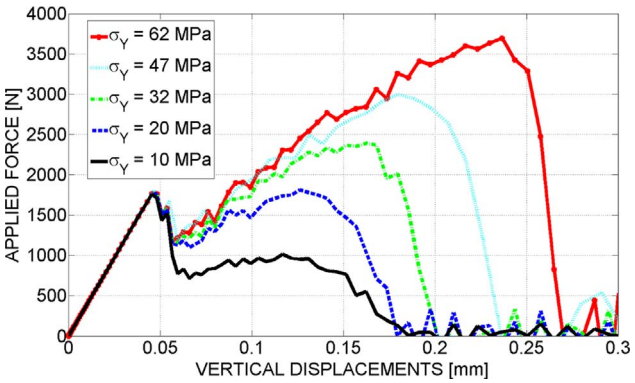

Fig. 7. Fully osseointegrated implant. The calculated resisting force versus the vertical displacement of the IS for five types of trabecular bones having yield stress of: 10, 20, 32, 47 and 62 MPa.

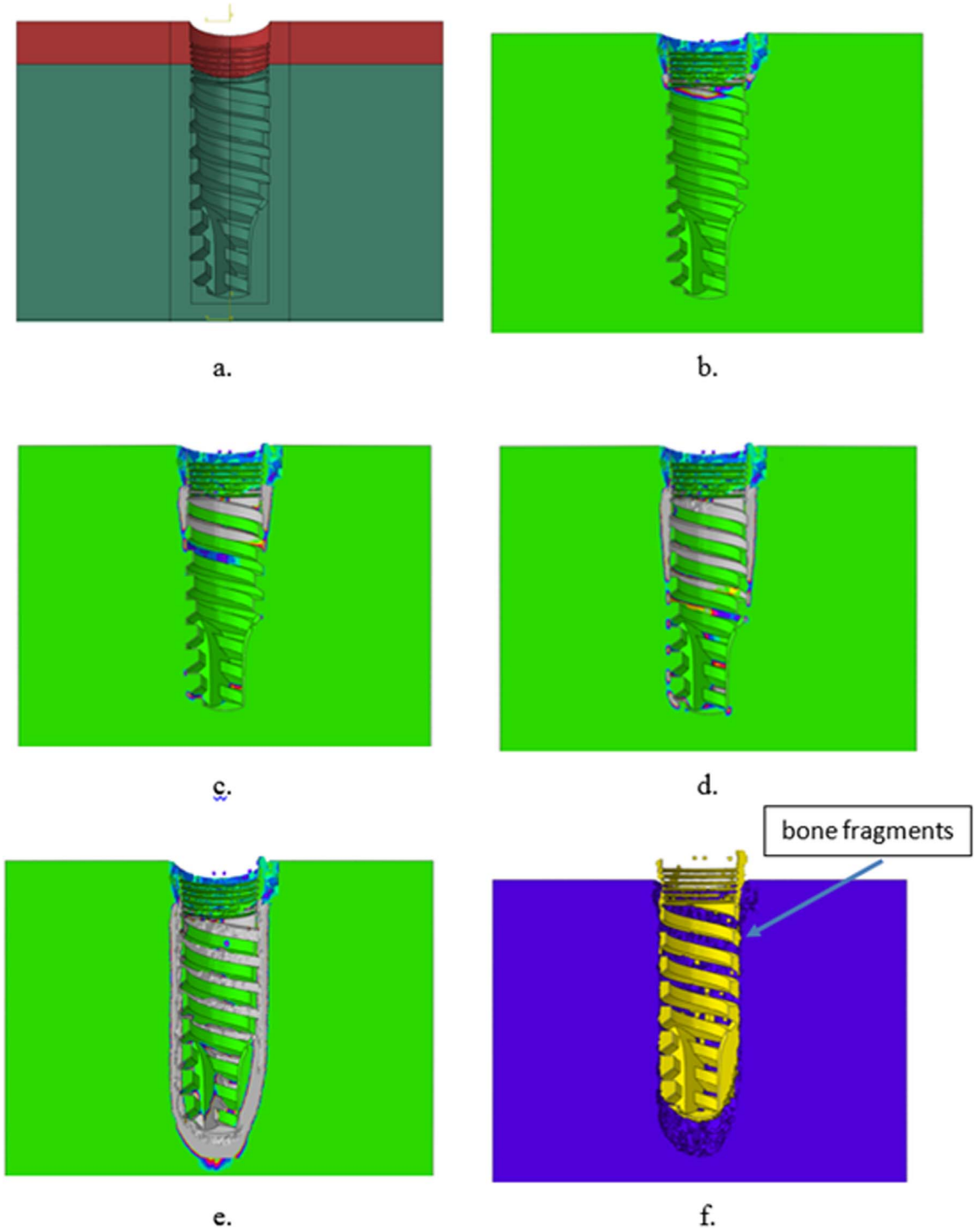

Fig. 8. A cross-sectional view through the bone showing plastic deformation at different stages during the extraction process of a fully osseointegrated implant. The stages are defined by the vertical applied displacement (vd) on IS. The trabecular bone has a yield strength of 32 MPa (cf. Fig. 7). a. Undeformed bone. b. Plastic deformation at vd = 0.06 mm. c. vd = 0.13 mm. d. vd = 0.16 mm. e. vd = 0.20 mm. f. Vertical displacement of torn bone at vd = 1.5 mm. Note that in figures b-e, the progressive damage zones have a color other than the green background. (For interpretation of the references to color in this figure legend, the reader is referred to the web version of this article).

pulling out a fully bonded titanium implant is calculated by application of Eq. (1) to the curves of Fig. 7. The work for unscrewing a fully bonded titanium implant is calculated by application of Eq. (2) to the curves of Fig. 9.

Fig. 11 shows that the higher the yield stress of the trabecular bone, the higher the work needed for extraction, which is intuitive. While the work due to the pullout forces is almost linear with the yield strength of the trabecular bone, the work of unscrewing shows a cubic dependence.

The average and maximum pullout forces are shown in Fig. 12a, while the average and maximum torque are shown in Fig. 12b.

The averaged values are based on the extraction (pullout or rotational) work (Fig. 11), and are obtained by dividing the integrated extraction work by the total displacement/angle results (Figs. 6, 7, 9).

Our results show that the maximum torque value or the maximum pullout force value are not the best parameters for assessing the interfacial strength, especially when two types of bones (cortical and

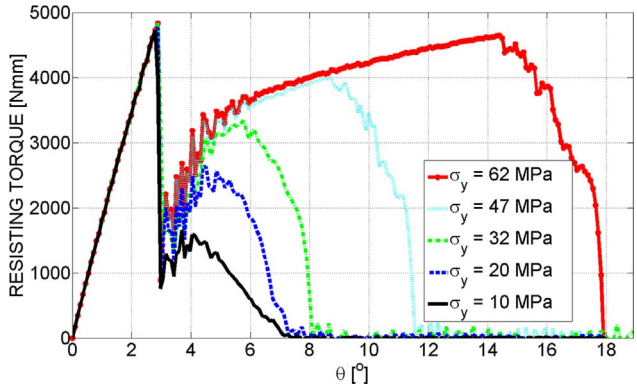

Fig. 9. The calculated resisting torque versus the rotation angle of the IS of the implant for five types of trabecular bones having yield stress of 10, 20, 32, 47 and 62 MPa.

trabecular) are involved, since the high cortical bone strength is causing a local extremum which does not really indicate about the gross interfacial strength.

3.3.2. Maximum extraction load – the effect of osseointegration

The maximum load for pullout is the usually reported value that is deemed to characterize the bone-implant interfacial strength. The ratio between the maximum and average pullout force, long after insertion (Fig. 7) to the maximum and average pullout force right after insertion (Fig. 6) respectively is shown in Fig. 13, as a function of trabecular bone yield stress. It is clear that for "strong" trabecular bones, for which $20 < \sigma_Y < 62$ MPa, this ratio lies between 2.8 and 3.9. For "weaker" trabecular bones, this ratio increases up to 9.7 for $\sigma_Y = 10$ MPa. One has to note that immediately after insertion, there is no contact between the implant neck and the cortical bone (Dorogoy et al., 2017), and it is the relatively weak trabecular bone which resists the pullout. When pulling out an implant long after insertion, there is a full bond between the implant neck and the "stronger" cortical bone. This bond must first be broken, and only thereafter, the trabecular bone starts to carry the load. Tearing the cortical bone-implant interface requires a significant force that is much higher than what the "weak" ($\sigma_Y < 20$ MPa) cortical bone can carry, hence the observed increase in the forces' ratio.

3.4. A parametric study of the force-displacement and the torque-angle relationships

In the sequel, we characterize the effect of the yield stress of the cortical bone, and the failure strain of the trabecular bone, on the torque and force variations during pullout of a fully bonded implant (as in Section 2.2), for a (constant) hard trabecular bone having $\sigma_Y = 62$ MPa. The yield stress of the cortical bone in compression is varied from 180 MPa to 90 MPa, and the failure strain of the trabecular bone from 0.135 to 0.270, in separate simulations.

Decreasing the yield stress from 180 MPa to 90 MPa has a similar effect on the torque (Fig. 14a) and the force (Fig. 15a), in the sense that the initial peak decreases significantly.

Likewise, increasing the failure strain of the trabecular bone from 0.135 to 0.27 allows for an "extended" response of the system in which larger maximum torque values (Fig. 14b) and pullout force (Fig. 15b) are reached. This comes along naturally with larger angle and displacement values to failure.

3.4.1. Discussion and conclusion

This paper is a continuation of our previous work on dental implant insertion (Dorogoy et al., 2017). It uses the available numerical simulation techniques to shed light on the two kinds of extraction processes: application of a force or a torque.

Literature survey reveals that there is no unique relationship between the torque-angle or force-displacement. This work aims at elucidating the dominant factors that dictate these measured relations.

Before reviewing the obtained results, the approach adopted here should be discussed. The bone-implant interaction occurs through their common interface. This can be modelled using two distinct approaches. The first approach consists of assigning specific mechanical and failure properties to the interface, as a third and distinct entity between the bone and the implant. However, such information is currently missing, even if the nature (as opposed to properties) of the interface have been extensively investigated through the bone to implant contact (BIC) concept.

The second approach adopted here consists of considering the interaction without defining a specific interface. The interaction can be frictional when no osseointegration has taken place yet (the early experiment), of assuming two perfectly bonded solids (after full osseointegration). It should be mentioned that full osseointegration is at best comprised of 80% bone to implant contact (BIC). It is thus clear that the assumption of perfect bonding leads to an upper limit kind of results, yet having the advantage that no ad-hoc models are used for the interface. In this case, the failure will always be of a cohesive nature, as evidenced by the observed bone fragments.

For a fixed implant and bone geometry, the main parameters of the bone-implant system are the respective strength and failure parameters of the cortical and trabecular bones, as well as the level of osseointegration reached. Note that those parameters are homogeneized values that do not account for density (thus strength) gradients inside the bone.

The immediate extraction load-displacement relationship was found to exhibit remarkably similar characteristics for a systematic variation of the trabecular bone yield strength. Likewise, the same generic trend was observed for the load-displacement and torque-angle relationships as a function of the trabecular bone strength during extraction of a fully bonded implant.

For immediate extraction, the damaged trabecular bone is the only component to resist extraction, since the insertion process has destroyed the cortical bone around the neck of the implant. The load-displacement curve exhibits a moderate increase up to 0.2–0.4 mm, followed by a moderate drop to zero at ~1.0–1.2 mm. For a fully bonded implant, the extraction process starts by failure of the cortical bone first, so that past a small displacement or angle, the implant motion is resisted by the trabecular bone only. Here, both the load and torque exhibit a local extremum due the resistance of the "strong" cortical bone. At failure of the cortical bone, the torque and load are partly released first, followed by an increase due to the resistance of the trabecular bone. The load drops to zero at a displacement of 0.18–0.27 mm.

The osseointegration effect on the extraction forces for bones having various strength was assessed by comparing the intensity of the peak extraction forces. This result shows that the ratio is quite high for low trabecular bone strength, but decreases significantly as the latter increases, to reach a stationary value of about 3. One has to note that for a "weak" ($\sigma_Y < 20$ MPa) trabecular bone, it is the cortical bone initial peak value that dictates the maximum load value, while during the rest of the extraction process, the resisting forces might be much lower. This fact raises some doubts on the peak extraction force as an indicator of the interfacial strength, when the interface is made of more than one type of bone.

As an alternative, we evaluated the work invested in each extraction process by integrating the load-displacement or torque-angle curves. Using this evaluation, the "efficiency" of each extraction procedure can be compared. It is interesting to note that all three procedures lead to approximately the same energy efficiency, which might be explained by the fact that irrespective of the procedure, the interfacial destruction process remains unaltered.

This approach was further pursued for calculating an average force or torque during the extraction process. Such an exercise, embodied in Fig. 12, might provide a better estimation for the interfacial strength

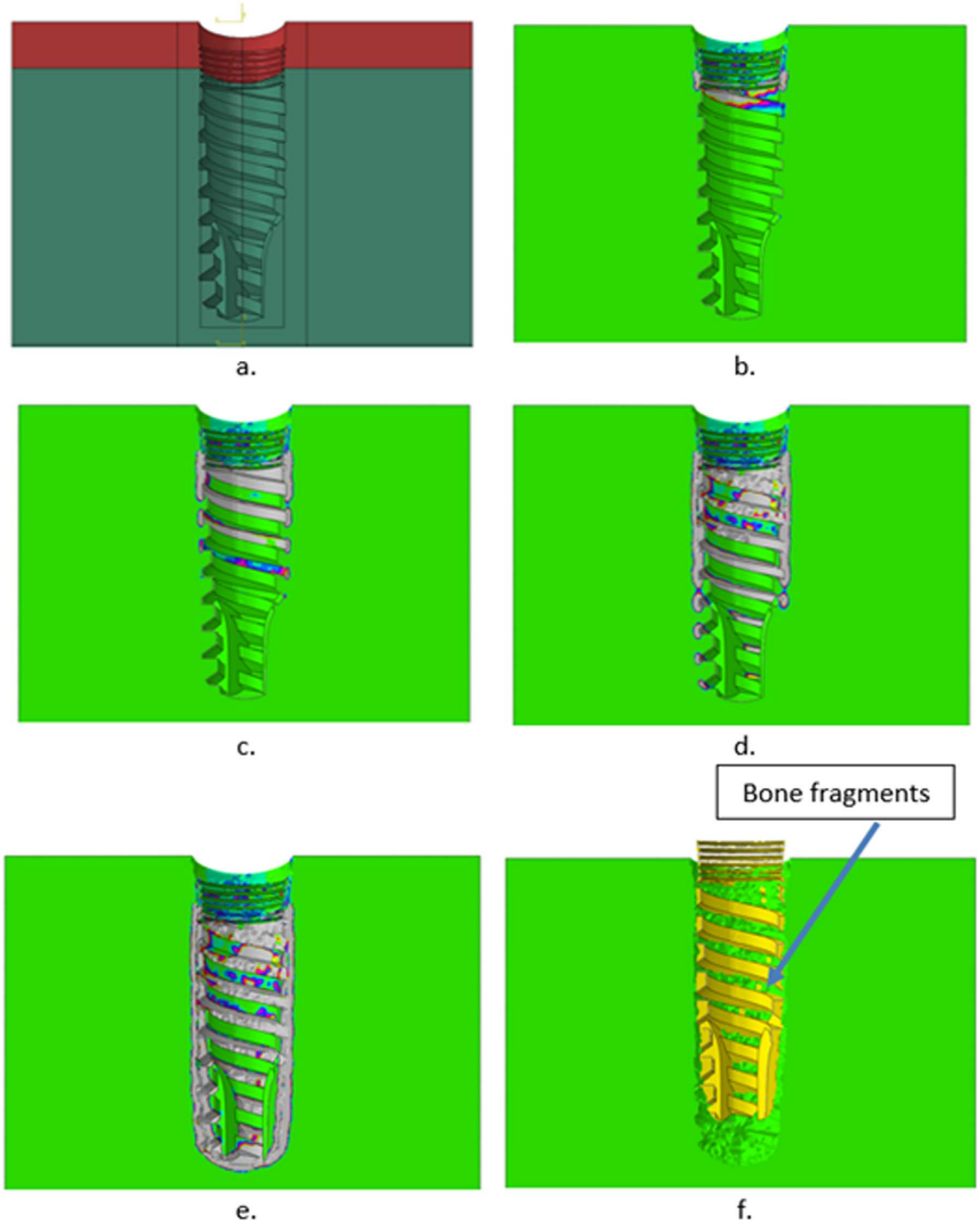

Fig. 10. A cross-sectional view through the bone showing it at different stages during the extraction process of a fully osseointegrated titanium implant. The stages are defined by the rotational angle (θ) applied on IS. a. Undeformed bone. b. Plastic deformation at θ = 3.2°., c. At θ = 5.0°., d. At θ = 6.8°, e. At θ = 8.3°. f. Vertical displacement of the ton bone at θ = 18°. The trabecular bone has $\sigma_Y = 32$ MPa, and the applied angular velocity is 30 rpm (cf. Fig. 9). Note the bone fragments which are attached to the implant in f. Note that in figures b-e, the progressive damage zones have a color other than the green background. (For interpretation of the references to color in this figure legend, the reader is referred to the web version of this article.)

when more than one type of bone exists along the interface, because it is less sensitive to local extremum values such as those created by the cortical bone for a weak trabecular bone.

An interesting point is that of the presence of an initial peak in the torque-angle and force-displacement relationships during extraction of a fully bonded implant. This peak is the result of the contrast in strength between the cortical and the trabecular bone, and as the two strengths come closer to each other, the peaks decrease noticeably. Such an observation can be a first indirect indication of the respective strength of the bone components.

Another outcome of the simulations is that when the failure strain of the trabecular bone increases, the whole calculated relationship extends, thereby reaching higher load and torque values, for higher displacement and rotation angles, respectively.

These numerical parametric studies indicate that the mechanical characteristics of the bone components will determine the mechanical

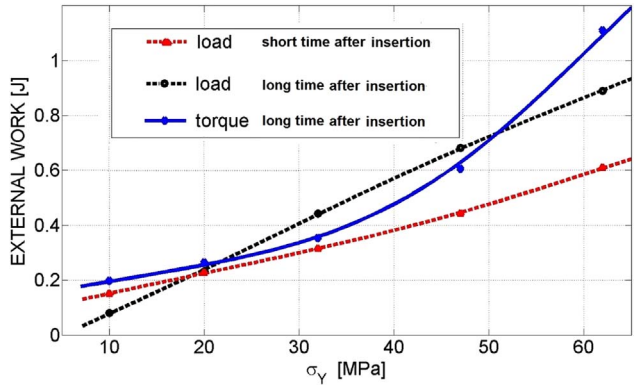

Fig. 11. The extraction work versus the yield stress of the trabecular bone for three scenarios: 1) Pullout immediately after insertion (immediate pullout), 2) Pull out of fully bonded implant (bonded pullout). 3) Unscrewing of a fully bonded implant (unscrewing bonded).

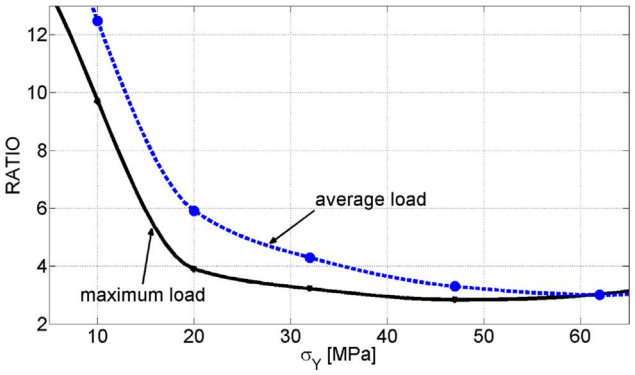

Fig. 13. Maximum long to short-term pullout force (average and maximum) ratios as a function of the trabecular bone yield stress. The stronger the trabecular bone, the smaller the contrast between the peak forces ratio.

response of the system.

If one tries to translate those observations into clinical terms, it can be claimed that the qualitative nature of the torque-angle or load-displacement relationships is a first indication of the relative mechanical properties of the bone components, including their contrast. If for example, the density of the cortical bone can be assessed, which can be translated into its strength, the presence and extent of mechanical peaks will immediately, yet qualitatively, reveal the mechanical state of the trabecular bone.

It can also be remarked that an extraction procedure, that would involve preliminary destruction of the peri-implant cortical bone would in principal eliminate the first peak (torque or vertical load), thus rendering the extraction procedure easier.

Simulations of the kind presented here can be run with a systematic variation of the material parameters until a reasonable resemblance between experimentally measured and numerically calculated relationships is obtained.

Our work indicates that adding modelling of the kind shown here to experimentally measured results should greatly assist in characterizing the bone-implant system and its interactions. It is also clear that additional experimental work, aimed at supplying the needed parameters and also measuring the presented calculated relationships will greatly complement the current numerical approach.

Acknowledgement

Mr. R. Korabi is kindly acknowledged for sharing his FE model of the commercial implant.

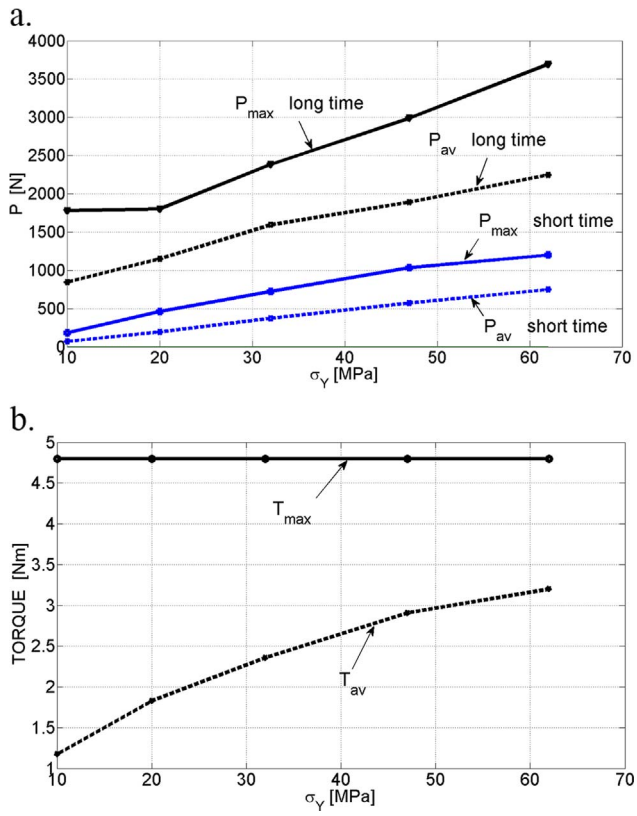

Fig. 12. a. The average extraction force versus the yield stress of the trabecular bone for pullout short time after insertion and pullout of fully bonded implant. b. The average extraction torque versus the yield stress of the trabecular bone for pullout of fully bonded implant.

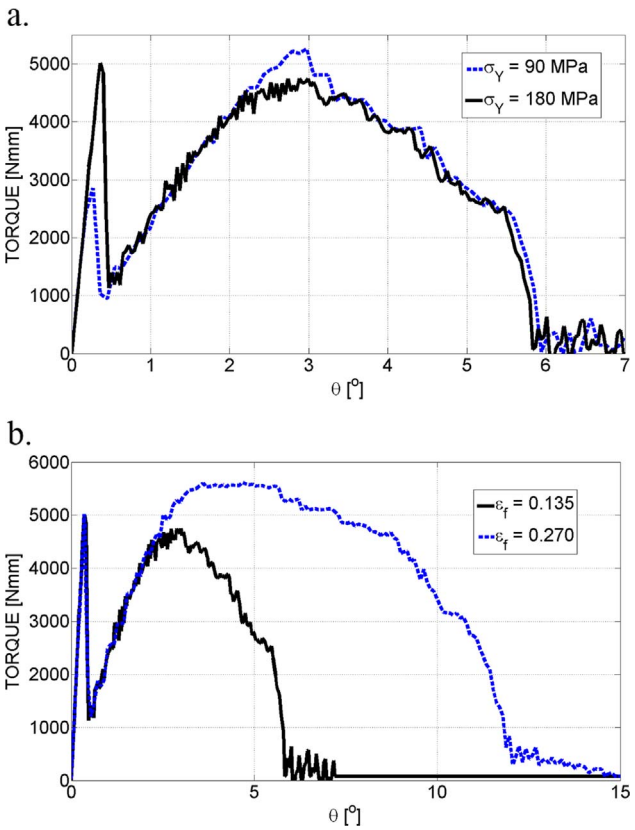

Fig. 14. Effect of material parameters on the pullout torque variation. a. Changing the cortical yield stress from 180 MPa to 90 MPa. b. Changing of the trabecular bone failure strain from 0.135 MPa to 0.270.

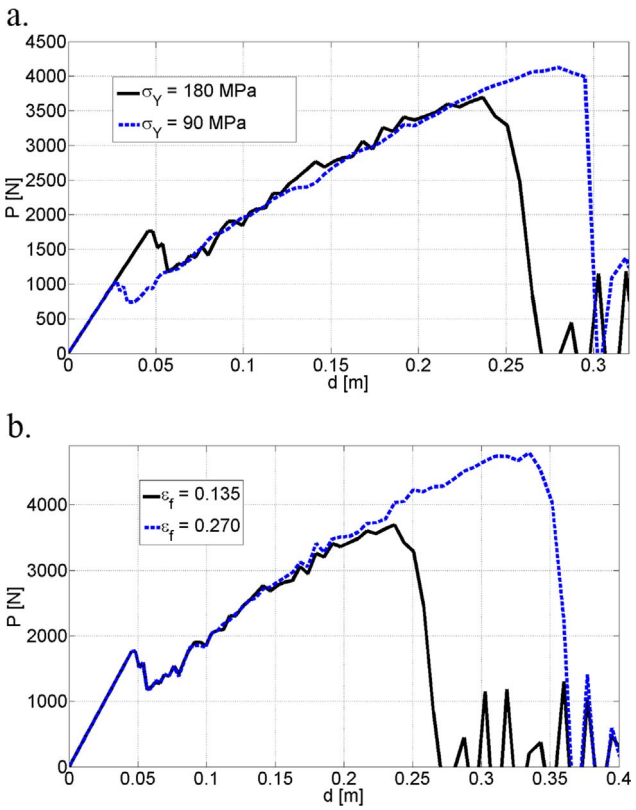

Fig. 15. Effect of material parameters on the pullout force variation. a. Changing of the cortical yield stress from 180 MPa to 90 MPa. b. Changing of the trabecular bone failure strain from 0.135 MPa to 0.270.

Appendix A. Geometry, mesh and boundary conditions for insertion and pullout

A1. Assembly dimensions

The implant is 3.75 mm diameter, 13 mm length, and it features 5 micro-rings on its neck. It has conical shape and threads that increase in thickness along the implant body, as shown in Fig. 1. The neck height is 3 mm, and the uppermost ~1 mm has no micro-rings.

A typical cross section of the mandible at the facial region was extruded 20 mm along the Z axis. It consists of cortical bone (grey in Fig. A1) having a thickness of ~2 mm, and of cancellous bone (green in Fig. A1). The overall dimensions are shown in Fig. A1b and A1c. An initial cylindrical cavity having a diameter 2.8 mm and depth of 13.3 mm was created. Since the neck outer diameter of the implant is 3.75 mm, the maximum diametrical misfit is of 0.95 mm between the implant and the pre-processed cavity.

A2. Mechanical properties of the model components

Implant: The implant was modeled as rigid material having a mass of 0.37 g.

Cortical bone: The cortical bone was modeled as an elastic plastic material with Drucker-Prager (DP) plasticity (Simulia, 2014a). Ductile failure with damage evolution (Simulia, 2014a) was used as a failure criterion. The tensile and compressive yield strengths were taken as 120 and 180 MPa, respectively. The plastic strain at fracture was set to 1%. in tension and 2% in compression (Keaveny and Hayes, 1992). The “damage evolution value”, expressing the residual displacement from attainment of the critical strain until final element deletion, was set to zero. It means that the failure of the cortical bone is considered to occur abruptly.

Cancellous bone: The cancellous bone is a cellular material (Ashby and Medalist, 1983), and is approximated here by an elastic-plastic material model with Mises plasticity (Simulia, 2014a). The Young's modulus, Poisson ratio and fracture strain were all taken from (Guan et al., 2011), while “representative” yield stresses were set to $10 < \sigma_Y < 62$ MPa. A failure strain of $\varepsilon_p^f = 0.135$ (Guan et al., 2011)was used with a small value of damage evolution of 10 μm.

The typical material properties, based on (Guan et al., 2011; Keaveny and Hayes, 1993; Reilly and Burstein, 1974; Van Staden et al., 2008) are summarized in Table A1. Note that perfect bonding was assumed between the cortical and trabecular bone components.

A3. Mesh

The implant was meshed with 8051 rigid elements: 7448 linear quadrilateral elements of type R3D4 and 603 linear triangular elements of type R3D3. The meshed implant is shown in Fig. A2a.

The bone was meshed with 858933 linear tetrahedral elements of type C3D4. The region around the cavity was meshed with small elements of size 0.2–0.3 mm, while the cortical bone around the cavity was made even denser, with a seed size of 0.1 mm as shown in Fig. A2b.

Numerical convergence was verified in preliminary calculations with different mesh sizes.

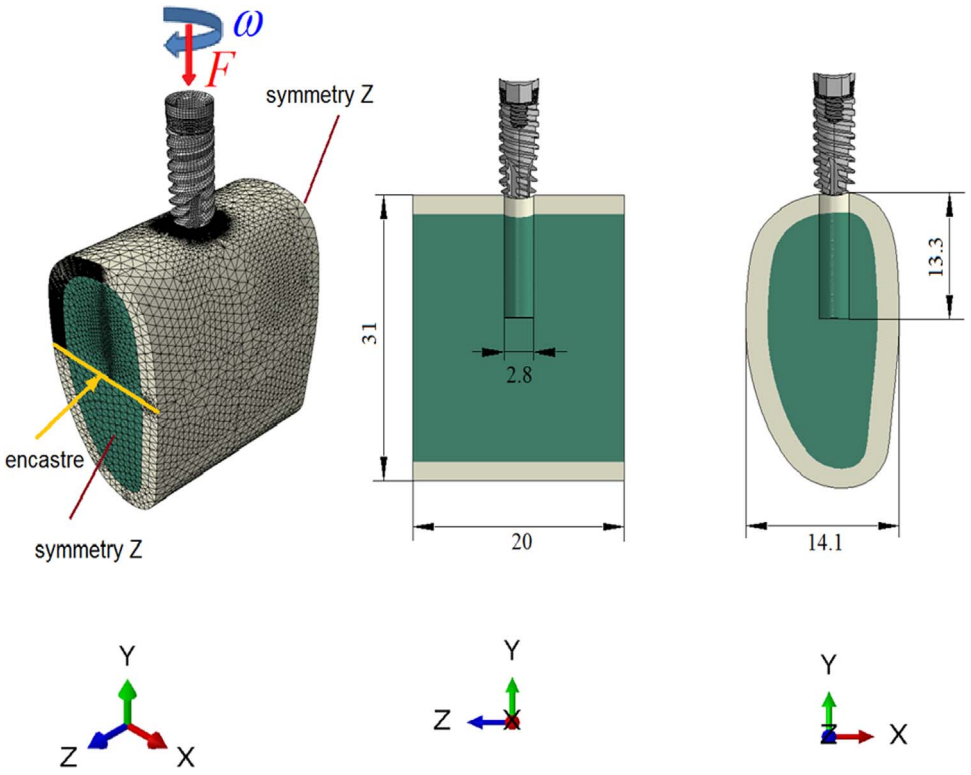

Fig. A1. Assembly of the implant and bone and boundary conditions at the beginning of the insertion process. a. Isometric view of the meshed assembly. b. Z-Y cross-sectional view. c. X-Y cross-sectional view. All dimensions are in mm.

Table A1
Material properties.

	ρ [Kg/m^3] density	E [MPa] Young's modulus	ν Poisson ratio	σ_Y [MPa] yield stress	β [°] Drucker Prager	ε_p^T [%] Fracture plastic strain tension	ε_p^C [%]Fracture plastic strain compression	Damage evolution [μm]
Cortical bone	1900	18,000	0.35	180	30	1	2	0.0
Cancellous bone	1000	700	0.35	10–62	0	0.135	0.135	10

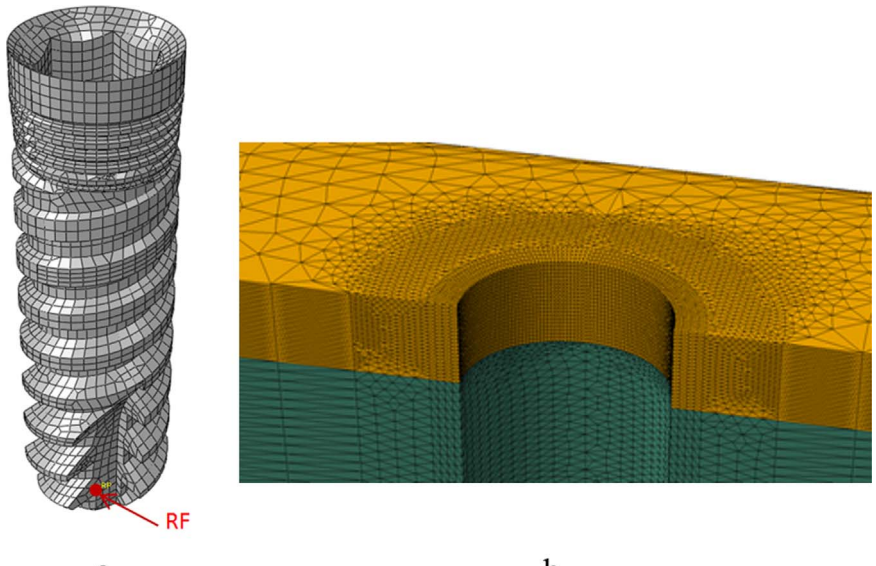

Fig. A2. a. The meshed implant. b. The mesh of the cortical bone around the hole. RF (reference point) indicates the point of application of vertical load and implant rotations.

A4. Boundary conditions

Symmetry conditions were applied on both planes of the bone with the normal pointing in the Z direction ($n_z = \pm 1$). A line along on the plane $n_z = \pm 1$ (Fig. A1a) was fixed in all directions to prevent rigid body motions of the assembly.

Only the boundary conditions on the implant change between the 3 analysis steps. During the insertion step the rigid implant was only allowed to rotate and move downwards in the y direction. A constant angular velocity (ω_y) of 120 rpm was applied as well as a constant downward force (F) of 5 N. They were applied on the reference point shown in Fig. A1a. The boundary conditions during the "rest" and "extraction" are detailed in Section 2.2.1.

References

Albrektsson, T., Hansson, H., Lindstrom, J., 1981. Osseointegrated titanium implants. Requirements for ensuring a long-lasting, direct bone-to-implant anchorage in man. Acta Orthop. Scand. 52, 155–170.

American Society for Testing and M., American Society for Testing and Materials, 2009. ASTM standard F543-07e1 standard specification and test methods for metallic medical bone screws 1–20. ⟨http://dx.doi.org/10.1520/F0543-13E01.Copyright⟩.

Ashby, M.F., Medalist, R.F.M., 1983. The mechanical properties of cellular solids. Metall. Trans. A 14, 1755–1769. http://dx.doi.org/10.1007/BF02645546.

Atsumi, M., Park, S., Wang, H., 2007. Methods used to assess implant stability: current status. Oral Maxillofac. Implant.

Brånemark, R., Öhrnell, L.-O., Skalak, R., Carlsson, L., Brånemark, P.-I., 1998. Biomechanical characterization of osseointegration: an experimental in vivo investigation in the beagle dog. J. Orthop. Res. 16, 61–69. http://dx.doi.org/10.1002/jor.1100160111.

Brånemark, R., Öhrnell, L.O., Nilsson, P., Thomsen, P., 1997. Biomechanical characterization of osseointegration during healing: an experimental in vivo study in the rat. Biomaterials 18, 969–978. http://dx.doi.org/10.1016/S0142-9612(97)00018-5.

Brunski, J.B., Puleo, D.A., Nanci, A., 2000. Biomaterials and biomechanics of oral and maxillofacial implants: current status and future developments. Int. J. Oral Maxillofac. Implant. 15, 15–46.

Chang, P.-C., Seol, Y.-J., Kikuchi, N., Goldstein, S.A., Giannobile, W.V., 2010. Functional apparent moduli as predictors of oral implant osseointegration dynamics. J. Biomed. Mater. Res. B. Appl. Biomater. 94, 118–126. http://dx.doi.org/10.1002/jbm.b.31631.

Chang, P.C., Lang, N.P., Giannobile, W.V., 2010a. Evaluation of functional dynamics during osseointegration and regeneration associated with oral implants. Clin. Oral Implant. Res. 21, 1–12. http://dx.doi.org/10.1111/j.1600-0501.2009.01826.x.

Chang, P.C., Seol, Y.J., Kikuchi, N., Goldstein, S.A., Giannobile, W.V., 2010b. Functional apparent moduli as predictors of oral implant osseointegration dynamics. J. Biomed. Mater. Res. B Appl. Biomater. 94, 118–126. http://dx.doi.org/10.1002/jbm.b.31631.

Dhert, W., Verheyen, C., Braak, L., 1992. A finite element analysis of the push-out test: influence of test conditions. Res. Part A.

Dorogoy, A., Rittel, D., Shemtov-Yona, K., Korabi, R., 2017. Modeling dental implant insertion. J. Mech. Behav. Biomed. Mater. 68, 42–50. http://dx.doi.org/10.1016/j.jmbbm.2017.01.021.

Ferguson, S.J., Langhoff, J.D., Vet, M., Voelter, K., 2008. Biomechanical comparison of different surface modifications biomechanical comparison of different surface. Int. J. Oral. Maxillofac. Implant. 23, 1037–1046.

Grant, J.A., Bishop, N.E., Götzen, N., Sprecher, C., Honl, M., Morlock, M.M., 2007. Artificial composite bone as a model of human trabecular bone: the implant-bone interface. J. Biomech. 40, 1158–1164. http://dx.doi.org/10.1016/j.jbiomech.2006.04.007.

Guan, H., van Staden, R.C., Johnson, N.W., Loo, Y.-C., 2011. Dynamic modelling and simulation of dental implant insertion process—a finite element study. Finite Elem. Anal. Des. 47, 886–897. http://dx.doi.org/10.1016/j.finel.2011.03.005.

Hansson, S., Löberg, J., Mattisson, I., Ahlberg, E., 2011. Global biomechanical model for dental implants. J. Biomech. 44, 1059–1065. http://dx.doi.org/10.1016/j.jbiomech.2011.02.002.

Hoshaw, S.J., Brunski, J.B., Cochran, G.V.B., 1994. Mechanical loading of Brånemark implants affects interfacial bone modeling and remodeling. Int. J. Oral Maxillofac. Implant. 9, 345–360.

Hou, S.-M., Hsu, C.-C., Wang, J.-L., Chao, C.-K., Lin, J., 2004. Mechanical tests and finite element models for bone holding power of tibial locking screws. Clin. Biomech. 19, 738–745. http://dx.doi.org/10.1016/j.clinbiomech.2004.04.012.

Hsu, C.-C., Chao, C.-K., Wang, J.-L., Hou, S.-M., Tsai, Y.-T., Lin, J., 2005. Increase of pullout strength of spinal pedicle screws with conical core: biomechanical tests and finite element analyses. J. Orthop. Res. 23, 788–794. http://dx.doi.org/10.1016/j.orthres.2004.11.002.

Hsu, C., Wang, J., Hou, S., Chao, C., Lin, J., 2003. Pushout strength of tibial locking screws: development of finite element models. J. Chin. Inst. Eng. 26, 817–823. http://dx.doi.org/10.1080/02533839.2003.9670836.

Huja, S.S., Litsky, A.S., Beck, F.M., Johnson, K.A., Larsen, P.E., 2005. Pull-out strength of monocortical screws placed in the maxillae and mandibles of dogs. Am. J. Orthod. Dentofac. Orthop. 127, 307–313. http://dx.doi.org/10.1016/j.ajodo.2003.12.023.

Keaveny, T., Hayes, W., 1993. Mechanical properties of cortical and trabecular bone. Bone.

Keaveny, T.M., Hayes, W.C., 1992. Mechanical properties of cortical and trabecular bone. Bone 285–344.

Kraut, R.A., Dootson, J., McCullen, A., 1991. Biomechanical analysis of osseointegration of IMZ implants in goat mandibles and maxillae. Int. J Oral Maxillofac. Implant. 6, 187–194.

Mathieu, V., Vayron, R., Barthel, E., Dalmas, D., Soffer, E., Anagnostou, F., Haiat, G., 2012. Mode III cleavage of a coin-shaped titanium implant in bone: effect of friction and crack propagation. J. Mech. Behav. Biomed. Mater. 8, 194–203. http://dx.doi.org/10.1016/j.jmbbm.2011.12.012.

Reilly, D.T., Burstein, A.H., 1974. The mechanical properties of cortical bone. J. Bone Jt. Surg. Am. 56, 1001–1022.

Simulia, 2014a. Abaqus/Explicit Version 6.14-2, Abaqus documentation. Dassault systemes, 2014.

Simulia, 2014b. Abaqus/CAE Version 6.14-2 (2014). Dassault Systèmes Simulia Corp., Providence, RI, USA.

Stanford, C.M., Keller, J.C., 1991. The concept of osseointegration and bone matrix expression. Crit. Rev. Oral Biol. Med. 2, 83–101.

Trisi, P., De Benedittis, S., Perfetti, G., Berardi, D., 2011. Primary stability, insertion torque and bone density of cylindric implant ad modum Branemark: is there a relationship? An in vitro study. Clin. Oral Implant. Res. 22, 567–570. http://dx.doi.org/10.1111/j.1600-0501.2010.02036.x.

Van Staden, R.C., Guan, H., Johnson, N.W., Loo, Y., Meredith, N., 2008. Step-wise analysis of the dental implant insertion process using the finite element technique. Clin. Oral Implant. Res. 19, 303–313. http://dx.doi.org/10.1111/j.1600-0501.2007.01427.x.